PERGAMON

Acta mater. 48 (2000) 3477–3487

Acta MATERIALIA

www.elsevier.com/locate/actamat

CREEP PROPERTIES OF Al_3Sc AND $Al_3(Sc, X)$ INTERMETALLICS

Y. HARADA† and D. C. DUNAND‡

Department of Materials Science and Engineering, Northwestern University, 2225 N. Campus Drive, Evanston, IL 60208-3108, USA

(Received 9 March 2000; received in revised form 2 May 2000; accepted 2 May 2000)

Abstract—A systematic creep study was undertaken for the binary intermetallic Al_3Sc and the ternary single-phase intermetallic $Al_3(Sc_{0.74}X_{0.26})$, where X is one of the transition-metals Ti, Y, Zr or Hf. Creep tests were conducted in the temperature range from 673 to 1200 K under a constant compressive stress ranging from 30 to 300 MPa. The binary Al_3Sc exhibits a stress exponent of 4.4–4.9 indicative of creep controlled by climb of dislocations. The activation energy for creep of Al_3Sc was 128 ± 6 kJ/mol, close to that for self-diffusion for pure aluminum, in agreement with the Cu_3Au rule, indicating that diffusion on the Al-sublattice is controlling. Ternary $Al_3(Sc_{0.74}X_{0.26})$ exhibits a decrease in creep rate by about one order of magnitude for Zr and Hf and by about two orders of magnitude for Ti and Y. For all ternary alloys, a stress exponent of 3.9–5.5 was observed, indicative of dislocation creep. Activation energies for creep of 202 ± 8 kJ/mol were found, showing that ternary substitution for scandium with transition metals affects diffusion on the Al sublattice.

Keywords: Mechanical properties; Creep; Intermetallic compounds; Bulk diffusion; Scandium; Microstructure

1. INTRODUCTION

Aluminum-rich intermetallic compounds based on trialuminides (e.g. Al_3Ti, Al_3Y, Al_3Zr, Al_3Hf) have been investigated recently [1–5], because of their low density, relatively high melting point, good oxidation resistance and potentially useful high-temperature strength. These trialuminides have non-cubic structures ($D0_{22}$ for Al_3Ti, $D0_{19}$ for Al_3Y, and $D0_{23}$ for Al_3Zr and Al_3Hf) and are brittle at room temperature. However, $(Al, X)_3Ti$ where Al is partially replaced by V, Cr, Mn, Fe, Co, Ni or Zn can be transformed to the cubic ordered $L1_2$ structure [1, 6] with better prospects for room-temperature ductility, as exemplified by boron-doped Ni_3Al. It has only been possible recently to demonstrate a small amount of ductility in bending experiments in such ternary trialuminides. Zhang *et al.* [7] reported that hot-isostatically pressed Al–8Cr–25Ti has some ductility, a finding verified by Schneibel *et al.* [8] on hot-extruded materials of the same composition.

Scandium trialuminide (Al_3Sc) is a binary stable $L1_2$ intermetallic with a very low density (3.03 Mg/m^3) because scandium is the lightest of all transition metals. Intermetallics with the $L1_2$ structure are expected to deform plastically by the generation, motion and multiplication of $\langle 110 \rangle$ superdislocations on $\{111\}$ planes. In fact, Fukunaga *et al.* [9] reported that superdislocations in Al_3Sc dissociate into two $a/3\langle 112 \rangle$ superpartials separated by a superlattice intrinsic stacking fault at room temperatures. Schneibel *et al.* [10], however, found that polycrystalline Al_3Sc is brittle, with a relatively low yield stress increasing with temperature from 77 to 500 K. Fracture was found to occur in a transgranular manner by cleavage, primarily on $\{011\}$ planes. The phenomena of anomalous yield stress was also observed by Fukunaga *et al.* [9].

The increasing need for aluminum alloys with good creep resistance at high homologous temperatures has intensified the search for alloying elements producing fine, stable precipitates [11]. Scandium stands out among other alloying elements for aluminum alloys [12] as it produces very fine, thermodynamically-stable, coherent Al_3Sc precipitates with very low coarsening rates [13]. At elevated temperatures where the Al_3Sc precipitates are sheared, the creep properties of the Al_3Sc phase dictate those of the alloy. Little research has however

† Present address: Mechanical Engineering Laboratory, Agency of Industrial Science and Technology, MITI, Tsukuba, Ibaraki, Ibaraki 305-8564, Japan.

‡ To whom all correspondence should be addressed.

PII: S1359-6454(00)00142-7

been performed on the mechanical properties of the pure Al_3Sc phase [1, 9, 10, 14, 15]. In particular, despite potential high-temperature applications for Al_3Sc as precipitates in aluminum alloys or in bulk form, the high-temperature mechanical properties of Al_3Sc are almost unexplored, with the exception of Refs [9] and [15] who measured stress–strain curves in the range 77–1073 K and Ref. [16] who reported microhardness and elastic modulus from 298 to 773 K. The purpose of the present study is to determine, for the first time, the general characteristics of creep deformation for the binary Al_3Sc and ternary $Al_3(Sc, X)$, where scandium is replaced by different transition elements.

2. EXPERIMENTAL PROCEDURES

Button ingots of Al_3Sc and $Al_3(Sc_{0.74}X_{0.26})$, where X was chosen as Ti, Y, Zr or Hf, were prepared by non-consumable electrode arc-melting on a water-cooled copper hearth under a purified argon atmosphere. Initial charges consisted of about 5 g of high-purity metals: 99.94 wt.% pure scandium from Stanford Materials (San Mateo, CA) and 99.99 wt.% pure aluminum from Johnson Matthey (Ward Hill, MA), with appropriate ternary additions of 99.999 wt.% pure titanium, 99.9 wt.% pure yttrium, 99.94 wt.% pure zirconium or 99.97 wt.% pure hafnium (all from Johnson Matthey). First, some titanium was melted in the arc furnace to getter residual oxygen and nitrogen from the chamber. Next, melting of the charge was performed four or more times, flipping the charge after each solidification to ensure complete mixing of the metals. The final ingots, which exhibited a weight loss of less than 0.2% as compared to the initial charge, were homogenized for 2 h in vacuum (10^{-4} Pa) at 1473 K. Their density was measured by Archimedes' method in distilled water.

Al_3Sc is a line-compound in equilibrium with Al or Al_2Sc for aluminum-rich and -poor compositions, respectively [17]. While small deviations from stoichiometry are unavoidable during processing, creep rates would be significantly affected for Al-rich compositions (the Al–Al_3Sc eutectic temperature is 933 K), but not for Al-poor compositions (the Al_3Sc–Al_2Sc peritectic temperature is 1593 K). It was thus decided to shift the binary Al_3Sc and ternary $Al_3(Sc, X)$ alloys to a slightly Al-poor composition (74.8 at.% and 74.5 at.% Al, respectively). Al_3Sc is an incongruently-melting compound and many incongruently-melting trialuminides tend to develop Kirkendall porosity [14, 15] upon homogenization of cast, segregated specimens. To prevent any errors in creep measurement due to porosity closing, specimens of all compositions were subjected to hot-isostatic-pressing (HIP), performed by Pressure Technology Inc. (Warminster, PA) at 1423 K under 200 MPa for 4 h in an argon atmosphere.

Optical metallographic studies of all alloys were performed in order to characterize their microstructure. Specimens were polished with SiC papers and 0.05 μm Al_2O_3 and subsequently etched with H_2O-10 vol.% HF. Energy dispersive X-ray spectroscopy (EDS), scanning electron microscopy (SEM), and wet chemical analysis (Luvak, Inc., Boylston, MA) were also performed to obtain bulk and phase compositions. Lattice parameters were determined using powder X-ray diffraction (XRD) and were calculated by a least-squares method using the JADE program (Materials Data Inc., Livermore, CA).

Melting points were measured by differential thermal analysis (DTA) with a heating and cooling rate of 10 K/min to a maximum temperature of 1723 K in a flowing argon atmosphere. A small piece of the specimen (~100 mg) for each HIPed alloys was used for analysis. The measurements were repeated two or three times for each specimen.

Cylindrical creep specimens were electrode-discharge-machined with their axes perpendicular to the surface of the ingot which had been in contact with the water-cooled copper hearth. Specimen size was approximately 8 mm in height and 4 mm in diameter. Constant-load compression creep tests were performed in air on the binary Al_3Sc and ternary Al_3Sc alloys in the temperature range from 673 to 1200 K within the stress range from 30 to 300 MPa. A superalloy creep cage translated tensile loads in the pull-rods to compressive stresses on the specimen. Frictional effects on the end-loaded specimens were minimized by using boron nitride coated alumina platens in the creep cage. Specimen temperature was measured in the three-zone furnace with a temperature stability of ± 1 K after a 60 min soak at the test temperature. Specimen strains were calculated from extensometric displacements measured using a linear variable differential transducer with a resolution of 2.5 μm. Six specimens of each composition were used for the creep study of homogenized ingots and four specimens for HIPed ingots. Because of the limited supply of specimens, multiple measurements were made on each specimen to obtain an activation energy (using increasing temperatures) and a stress exponent (using increasing stresses).

3. RESULTS

3.1. Microstructure

X-ray diffraction from powder specimens confirmed that the binary Al_3Sc has the $L1_2$ structure with a lattice parameter $a = 4.1026(7)$ Å, in good agreement with previous results [9]. The bulk composition was 74.8 at.%Al–25.2 at.%Sc as measured by wet chemical analysis. The melting point was $T_M = 1586 \pm 3$ K and the density was $\rho = 3.024 \pm 0.007$ Mg/m^3. Grains with somewhat columnar shape were observed, with their long axis perpen-

dicular to the water-cooled copper hearth, resulting from the temperature gradient present during solidification. The average grain size is 0.57 and 0.71 mm on planes perpendicular and parallel to the copper hearth, respectively. While the structure of homogenized Al_3Sc is predominantly single-phase, small volume fractions of voids (typically 5 μm) and precipitates (5 μm) were observed in the grain interiors. The voids are most likely Kirkendall porosity: incongruent solidification of a melt with Al_3Sc overall composition produces a mixture of Al_2Sc and Al–Al_3Sc eutectic [17], which, upon homogenization, leads to single-phase Al_3Sc, albeit with Kirkendall porosity due to the high diffusivity of Al. The second phases are attributed to the fact that Al_3Sc is a line compound and the composition was slightly off-stoichiometric. The globular precipitates in the grain interior were indeed identified as scandium-enriched phases by EDS analysis. In contrast, the microstructure of HIPed Al_3Sc (Fig. 1) showed reduced porosity with no visible second phases and no significant change in grain size (0.46 and 0.89 mm). Although some oxygen contamination was expected from oxides present in the pure metals, the oxygen content of Al_3Sc was fairly low (0.0035 wt.%).

The as-cast ternary alloys exhibit a segregated microstructure consisting of a single majority phase with a low volume fraction of grain boundary phase and a few second phase particles scattered in the grain interiors. These phases are expected to be $Al_3(Sc, X)$, Al and $Al_2(Sc, X)$, respectively, as a result of segregation from the rather high solidification rate of the alloy. The Al-phase disappeared after the homogenization treatment but, as expected, significant Kirkendall porosity developed. For the Zr-containing alloy, the XRD and EDS analysis confirmed that the matrix had the $L1_2$ structure with a composition of $Al_3(Sc_{0.74}Zr_{0.26})$, ignoring the small deviation from stoichiometry discussed above. The average grain size is approximately 0.40 and 0.47 mm on planes perpendicular and parallel to the copper hearth. Precipitates (30 μm) as well as Kirkendall porosity (30 μm) in the grain interior are observed. The globular precipitates in the grain interior are Sc-enriched phases identified by EDS and XRD as $Al_2(Sc,Zr)$ with the C15 crystal structure. The microstructure of HIPed $Al_3(Sc_{0.74}Zr_{0.26})$ shown in Fig. 2 has smaller porosity (5 μm) and precipitates (10 μm) in grain interiors than for the homogenized alloy. The grain size was unchanged (0.45 and 0.56 mm).

Optical micrographs of HIPed $Al_3(Sc_{0.74}Ti_{0.26})$, $Al_3(Sc_{0.74}Y_{0.26})$ and $Al_3(Sc_{0.74}Hf_{0.26})$ were similar to that of HIPed $Al_3(Sc_{0.74}Zr_{0.26})$ shown in Fig. 2. $Al_3(Sc_{0.74}Ti_{0.26})$ has a small porosity (~5 μm) in the grain interiors and is essentially single phase. The average grain size is approximately 0.36 and 0.65 mm on planes perpendicular and parallel to the copper hearth. $Al_3(Sc_{0.74}Y_{0.26})$ has small pores not only in the grain interiors (~5 μm) but also at grain boundaries (20 μm). In addition, precipitates (50 μm, $Al_2(Sc, Y)$) are seen. The grain sizes are 0.32 and 0.55 mm. For $Al_3(Sc_{0.74}Hf_{0.26})$, small porosity (~5 μm) in the grain interiors and some Sc-rich grain boundary phases ($Al_2(Sc, Hf)$) appear. The grain sizes are 0.24 and 0.51 mm.

Table 1 summarizes the physical and microstructural characteristics of the binary Al_3Sc and ternary $Al_3(Sc, X)$ alloys. Density measurements demonstrate that homogenized specimens before HIP treatment have a density of $99.80 \pm 0.10\%$ of the theoretical value of 3.03 Mg/m^3 for Al_3Sc [9]. For $Al_3(Sc, X)$, the density increases with that of the transition metal and it also slightly increases after HIP treatment (the increase is systematic in all cases, but still within measurement error). Density changes after creep are within experimental error. Optical microscopy revealed that there is no evidence of grain coarsening in the creep-tested specimens. The lattice parameter increases with Y concentration, but decreases with Ti, Zr or Hf additions, which were all below the solubility limit of $L1_2$ Al_3Sc. Also, the melting point increases with

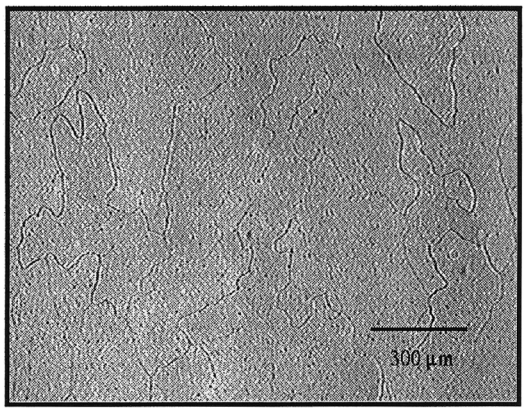

Fig. 1. Micrograph of HIPed Al_3Sc.

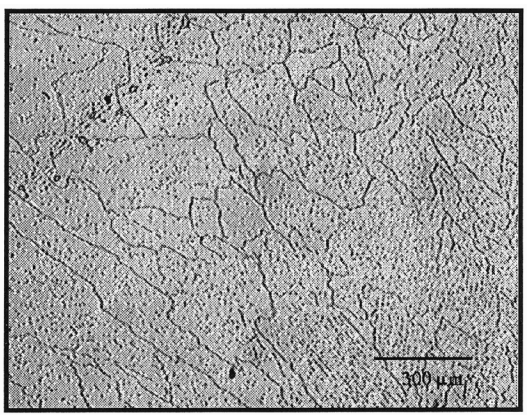

Fig. 2. Micrograph of HIPed $Al_3(Sc_{0.74}Zr_{0.26})$.

Table 1. Experimental physical and microstructural characteristics of Al_3Sc and $Al_3(Sc, X)$ alloys

Specimen	Heat treatment[a]	Crystal structure	Grain size[b]/mm		Density/Mg/m^3			Melting point/K	Lattice parameter/Å		Oxygen content/wt ppm
			On planes perpendicular to hearth	On planes parallel to hearth	Before HIP	After HIP	After creep				
Al_3Sc	Homogenized	$L1_2$	0.08–1.20 (0.57)	0.10–2.10 (0.71)	3.024(7)	–	3.024(4)	–	4.1026 (7)		–
$Al_3(Sc_{0.74}Zr_{0.26})$	Homogenized	$L1_2(+C15(Al_2Sc))$	0.06–1.00 (0.40)	0.09–1.20 (0.47)	3.328(11)	–	3.331(2)	–	–		–
Al_3Sc	Homogenized + HIPed	$L1_2$	0.10–1.20 (0.46)	0.18–2.70 (0.89)	3.024(7)	3.024(3)	3.026(2)	1586(3)	–		350
$Al_3(Sc_{0.74}Ti_{0.26})$	Homogenized + HIPed	$L1_2$	0.10–0.90 (0.36)	0.09–2.00 (0.65)	3.108(4)	3.115(6)	3.117(8)	1559	4.0701(10)		410
$Al_3(Sc_{0.74}Y_{0.26})$	Homogenized + HIPed	$L1_2(+C15)$	0.08–0.72 (0.32)	0.08–1.30 (0.55)	3.179(11)	3.184(13)	3.197(14)	1497(3)	4.1338(16)		710
$Al_3(Sc_{0.74}Zr_{0.26})$	Homogenized + HIPed	$L1_2(+C15)$	0.16–1.00 (0.45)	0.08–1.40 (0.56)	3.328(11)	3.329(11)	3.327(10)	1621(1)	4.0937(10)		530
$Al_3(Sc_{0.74}Hf_{0.26})$	Homogenized + HIPed	$L1_2(+C15)$	0.04–1.20 (0.24)	0.06–1.80 (0.51)	3.875(9)	3.878(5)	3.882(4)	1601(3)	4.0887(10)		340

[a] Homogenized: 1473 K/2 h, HIP: 1423 K/4 h/200 MPa.
[b] Range and, in parentheses, average.

addition of Zr (by 35 K) and Hf (by 15 K), but decreases with addition of Ti (by 27 K) or Y (by 89 K). Oxygen contents measured by chemical analysis were fairly low and $Al_3(Sc_{0.74}Y_{0.26})$ had the highest oxygen content (710 wt. ppm).

3.2. Creep behavior of homogenized Al_3Sc and $Al_3(Sc_{0.74}Zr_{0.26})$

Given the very coarse grain size for all specimens, grain boundary diffusional creep can be neglected and creep deformation can be assumed to result primarily from dislocation mechanisms. The minimum creep rate, $\dot{\varepsilon}$, can be described by a power-law:

$$\dot{\varepsilon} = A\left(\frac{\sigma}{E(T)}\right)^n \exp\left(-\frac{Q}{RT}\right) \qquad (1)$$

where A is a material constant, σ is the applied stress, E is the Young's modulus, n is the stress exponent, Q is the activation energy for creep, R is the gas constant and T is the absolute temperature. The minimum creep rate was reached after a very short primary stage (e.g. about 0.1–0.3% at 873–1073 K and 70 MPa).

Figure 3(a) and (b) shows the stress dependence of the minimum creep rate for homogenized Al_3Sc and $Al_3(Sc_{0.74}Zr_{0.26})$, respectively. Figure 3(a) illustrates that the stress exponent of the binary Al_3Sc decreases with increasing temperatures (from n = 4.9 at 673 K to n = 4.7 at 773 K, to n = 4.4 at 873–1073 K). On average, the stress exponent is approximately 4.5, which is characteristic of dislocation creep in metallic systems. Figure 3(b) shows that, for ternary $Al_3(Sc_{0.74}Zr_{0.26})$, the stress exponent is about 5.2 at 873 K and decreases to 4.4 at 973 K and 1073 K. The minimum creep rate is much smaller than that for binary Al_3Sc, demonstrating the effect of solid-solution strengthening by partially substituting Zr for Sc.

Apparent activation energies for creep deformation were obtained from the slope of semi-logarithmic Arrhenius plots of strain rate vs inverse temperature. The activation energy for the binary Al_3Sc is 124–134 kJ/mol (on average, 128 ± 6 kJ/mol) over the stress range 70–200 MPa. These

Table 2. Experimental activation energies for Al_3Sc and $Al_3(Sc, X)$ alloys

Alloys	Q/kJ/mol			
	70 MPa	100 MPa	150 MPa	200 MPa
Al_3Sc (homog.)	134	128	126	124
(HIPed)	137	152	152	136
$Al_3(Sc_{0.74}Ti_{0.26})$ (HIPed)	–	212	207	205
$Al_3(Sc_{0.74}Y_{0.26})$ (HIPed)	–	225	206	192
$Al_3(Sc_{0.74}Zr_{0.26})$ (homog.)	–	208	207	197
(HIPed)		203	201	197
$Al_3(Sc_{0.74}Hf_{0.26})$ (HIPed)	–	203	197	187

values are slightly stress dependent (Table 2). The activation energy for ternary $Al_3(Sc_{0.74}Zr_{0.26})$ over the stress range 100-200 MPa is 197–208 kJ/mol (204 ± 7 kJ/mol, Table 2). There is thus a significant increase in the apparent activation energy with zirconium substitution.

3.3. Creep behavior of HIPed Al_3Sc and $Al_3(Sc_{0.74}X_{0.26})$ alloys

Figures 4(a)–(e) shows the stress dependence of the minimum creep rate at 873, 973 and 1073 K for binary Al_3Sc and ternary $Al_3(Sc, X)$ after homogenization and HIP treatment. Also plotted for comparison in Fig. 4 is the creep rate for homogenized Al_3Sc. As shown in Fig. 4(a), the creep rates for homogenized Al_3Sc before and after the HIP treatment are the same, indicating that the small amounts of porosity found after homogenization had no influence on the creep rate of the binary alloy. Because of the smaller data set, activation energy for HIPed Al_3Sc shows more variation with stress than for homogenized Al_3Sc (Table 2).

The stress dependence of the minimum creep rate for HIPed $Al_3(Sc_{0.74}Ti_{0.26})$ is shown in Fig. 4(b). Upon long exposure times at 1073 K, this alloy formed a thick oxide layer (several tenths of a millimeter in thickness), thus preventing accurate measurements of creep rates at low strain rates. The low-stress creep tests at 1073 K were thus performed under flowing argon gas. The minimum creep rate for $Al_3(Sc_{0.74}Ti_{0.26})$ is approximately two orders of magnitude smaller than that for binary Al_3Sc and the stress exponent varies between 5.4 and 4.6 and is thus comparable to binary Al_3Sc.

Figure 4(c) shows the stress dependence of the minimum creep rate for HIPed $Al_3(Sc_{0.74}Y_{0.26})$. The creep rates are similar to those measured for $Al_3(Sc_{0.74}Ti_{0.26})$ and are thus much lower than for binary Al_3Sc. The stress exponent is about 5.5, decreasing to 4.4 at higher temperatures. Figure 4(d) gives the stress dependence of the minimum creep rate for HIPed $Al_3(Sc_{0.74}Zr_{0.26})$, which are the same, within experimental error, as those of homogenized $Al_3(Sc_{0.74}Zr_{0.26})$, also shown in Fig. 3(b). While the larger porosity detected in these materials was suspected to affect creep rates by densification during creep testing, no measurable effect was found, as for binary Al_3Sc. Two creep tests were performed at 1073 K under flowing argon gas, but no significant change in creep rates were found as compared to tests performed in air, as expected from the very thin oxide layer observed after high-temperature exposure.

Finally, Fig. 4(e) shows the stress dependence of the minimum creep rate for HIPed $Al_3(Sc_{0.74}Hf_{0.26})$. The creep rates are similar to those for $Al_3(Sc_{0.74}Zr_{0.26})$ and approximately one order of magnitude lower that for binary Al_3Sc. However, the stress exponent is slightly smaller that for the binary alloy and varies from 4.4 at 873 K to 3.9 at 1073 K.

The slope of Arrhenius plots for HIPed ternary alloys gave activation energies of about 202 ± 6 kJ/mol (Table 2) which are nearly independent of stress in the investigated range (100–200 MPa) and of the alloying element. There is however a significant increase in the activation energy as compared to the binary Al_3Sc alloy ($Q = 128 \pm 6$ kJ/mol).

4. DISCUSSION

4.1. Creep behavior of binary and ternary Al_3Sc alloys

The stress exponents of the ternary alloys are

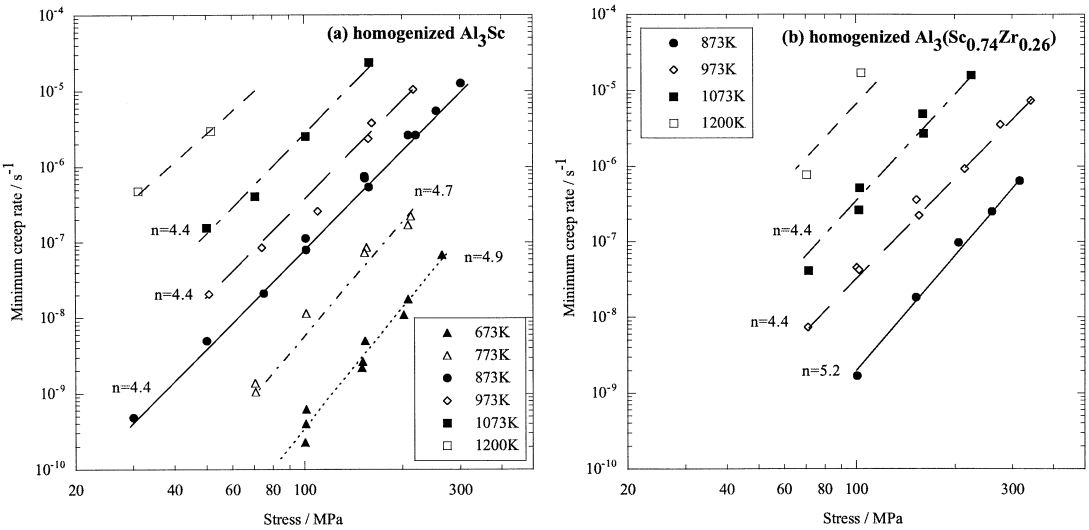

Fig. 3. Stress dependence of the minimum creep rate for homogenized (a) Al_3Sc and (b) $Al_3(Sc_{0.74}Zr_{0.26})$.

close to that for the binary intermetallic (Table 3), indicating that the main deformation mechanism (dislocation creep) is unchanged. The value of the stress exponent is close to five and the presence of a normal primary creep stage (decreasing creep rate with time) both suggest that the creep behavior of binary and ternary Al_3Sc alloys follow class II behavior (dislocation climb control), as observed in pure metals and many disordered solid solution alloys [18]. As no other information exists in the literature about the creep properties of Al_3Sc alloys, our results cannot be directly compared with other experimental data. Comparing with other $L1_2$ compounds, the stress exponent is similar to values of n

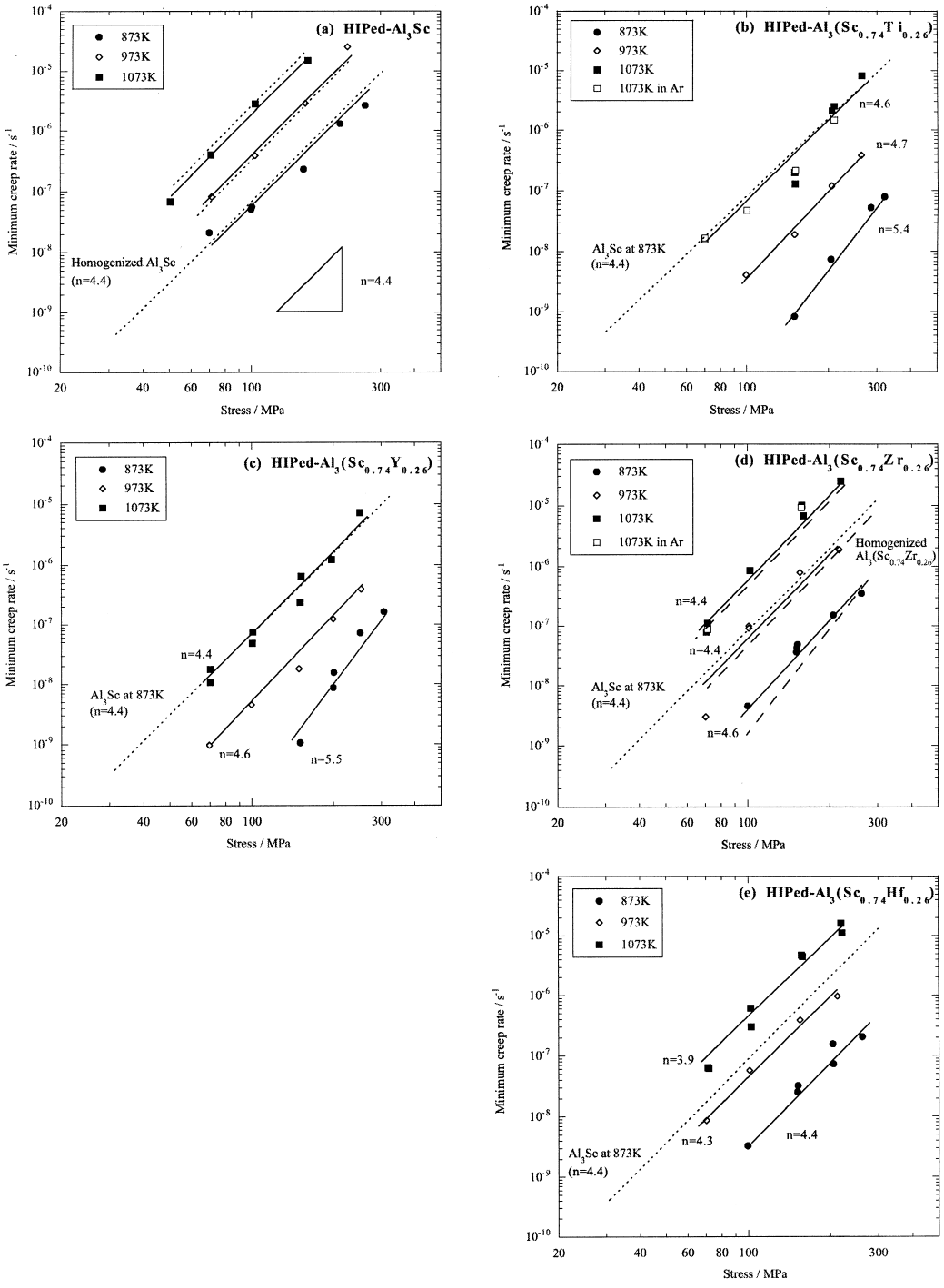

Fig. 4. Stress dependence of the minimum creep rate for (a) Al_3Sc, (b) $Al_3(Sc_{0.74}Ti_{0.26})$, (c) $Al_3(Sc_{0.74}Y_{0.26})$, (d) $Al_3(Sc_{0.74}Zr_{0.26})$ and (e) $Al_3(Sc_{0.74}Hf_{0.26})$, after homogenization and HIP treatment.

= 4.4 for Ni_3Al(Zr, B) reported by Wolfenstine *et al.* [19], n = 4.3 reported by Hemker and Nix for single crystalline Ni_3Al [20] and n = 5 reported by Schneibel *et al.* for $(Al, Cr)_3Ti$ [8]. It is however in disagreement with values of n = 3–4 reported by Hayashi *et al.* for Ni_3Al with ternary transition-metal additions [21], which show Class I creep behavior, and with the value of n = 2.8 reported by Whittenberger *et al.* for $(Al, Fe)_3Ti$ [22].

A comparison of the creep behavior between binary and ternary alloys, shown in Fig. 5(a) at 873 K, reveals that, as compared to binary Al_3Sc, the creep rate of ternary alloys, at a given stress, is lowered by about one order of magnitude for Zr and Hf additions and by about two orders of magnitude for Ti and Y additions. An equivalent observation is that binary Al_3Sc has the same creep strength at 873 K as ternary alloys with Ti or Y at 1073 K (corresponding to a temperature advantage of 200 K) or as ternary alloys with Zr or Hf additions at 973 K (corresponding to a temperature advantage of 100 K). The same trend is observed in the creep behavior at 973 K and 1073 K as shown in Figs 5(b) and (c), but the relative differences decrease with increasing temperatures because of the higher activation energies of the ternary alloys. Comparing the strengthening effect at equal mass density, the ranking in terms of increasing strengthening efficiency is Hf, Zr, Y and Ti.

The exact mechanism responsible for this significant solid-solution strengthening needs to await precise observations of dislocations in crept specimens, but many factors may be operating, e.g. interaction of solute atoms with vacancies and dislocation jogs, segregation on stacking faults and increase of the Peierls stress. An interesting observation is that the decrease in creep rate correlates well with the lattice parameter change as compared with binary Al_3Sc, as expected if first-order elastic interactions occur between dislocations and solute atoms. The magnitude of the lattice parameter change $|\Delta a/a|$ is 0.2 and 0.3% for Zr and Hf (which induce a creep-rate decrease by about one order of magnitude), and 0.7 and 0.8% for Y and Ti (with a creep-rate decrease of about two orders of magnitude).

Creep data for different temperatures can be compared by plotting equation (1) in a dimensionless manner as $\dot{\varepsilon}\ \exp(Q/RT)/A$ vs $\sigma/E(T)$. Figure 6 shows such a normalized plot, where the temperature-dependent Young's modulus $E(T) = E_0 - (\partial E/\partial T)T$ was assumed to be the same for all alloys. We used $\partial E/\partial T = -0.026$ GPa K^{-1} as reported by Drits *et al.* [16] and $E_0 = 166$ GPa as reported at room temperature by Refs [1, 23]. With A and Q as fitting parameters for each alloy, Fig. 6 shows that data for all binary and tertiary alloys can be fitted reasonably well with n = 5.0.

4.2. Activation energy for creep deformation

As listed in Table 2, the apparent activation energies for creep are Q = 128 kJ/mol for homogenized, binary Al_3Sc and Q = 202 kJ/mol for the average of all HIPed ternary alloys. As shown by Barrett *et al.* [24], the creep activation energy can be corrected to take account for the temperature-dependence of the elastic modulus. This correction factor is however less than 8 kJ/mol and does not explain the large difference of 74 kJ/mol between the binary and ternary alloys.

Table 4 summarizes activation energies for some trialuminides and some pure metals. The activation energy for binary Al_3Sc is close to that of self-diffusion for pure aluminum [25]. This is in agreement with the "ordered Cu_3Au rule" [26] which states that, in intermetallic compounds of type A_mB_n with m/n greater than two, the fastest diffusion occurs with the majority element A on the A sublattice. In the A_3B compounds (which include the $L1_2$ structure), the majority element A atoms have eight A atoms and four B atoms as nearest neighbors, so that A atoms can easily exchange sites with A vacancies without destroying the symmetry of the structure. On the other hand, the minority B atoms are surrounded exclusively by A atoms and can diffuse only by exchange with A vacancies, thus breaking the symmetry of the structure. In compounds where elements of the majority atoms form a continuous network such A_3B, the diffusion of A atoms should thus have characteristics approaching those of the pure element A. As shown in Table 4, the creep activation energy for Al_3Sc (Q = 128 kJ/mol) is comparable to that for self-diffusion of aluminum (Q = 120–142 kJ/mol) and thus follows the Cu_3Au rule. Other trialuminides Al_3X listed in Table 4 have somewhat higher activation energies (Q = 156–184 kJ/mol) [27–32] but are also much closer to the activation energy of aluminum than of X, independently of their crystal structures. The Cu_3Au rule also holds for other $L1_2$ intermetallics:

Table 3. Experimental creep parameters for homogenized Al_3Sc and HIPed $Al_3(Sc, X)$ alloys

Alloys	Temperature range/K	Stress range/MPa	Stress exponent, n	Activation energy, Q/kJ/mol
Al_3Sc	673–1200	30–300	4.4–4.9	128(6)
$Al_3(Sc_{0.74}Ti_{0.26})$	873–1073	70–300	4.6–5.4	208(4)
$Al_3(Sc_{0.74}Y_{0.26})$	873–1073	70–300	4.4–5.5	208(17)
$Al_3(Sc_{0.74}Zr_{0.26})$	873–1200	70–300	4.4–5.2	200(3)
$Al_3(Sc_{0.74}Hf_{0.26})$	873–1073	70–250	3.9–4.4	196(6)

Ni_3Al ($Q \approx 300$ kJ/mol) [21, 25], Ni_3Ge ($Q = 258 \pm 2$ kJ/mol) and Ni_3Ga ($Q = 259 \pm 12$ kJ/mol) [33] all have activation energies close to that for nickel self-diffusion (Q = 278–293 kJ/mol [25, 34]), and Co_3Ti (Q = 260–361 kJ/mol [35]) is close to pure cobalt (Q = 288 kJ/mol [25]).

Table 3 shows that the addition of the ternary alloying elements to Al_3Sc increases the creep activation energy by about 74 kJ/mol as compared to binary Al_3Sc. Because these alloying elements partition to the Sc sublattice, they should not affect directly the diffusion on the Al sublattice, which controls the overall creep activation energy, as discussed above. As reported in Table 1, however, the ternary elements change the lattice constant of Al_3Sc and thus indirectly affect the Al sublattice by straining it, thus potentially affecting the concentration and mobility of vacancies on the Al sublattice. Another indication that the effect of the alloying elements is indirect is that the activation energy of ternary alloys is the same for all four alloying elements, despite large differences in their self-diffusion activation energies (e.g. 170 kJ/mol for α–Ti [25] and 360 kJ/mol for α–Hf [25]), and differences in valence and atomic size.

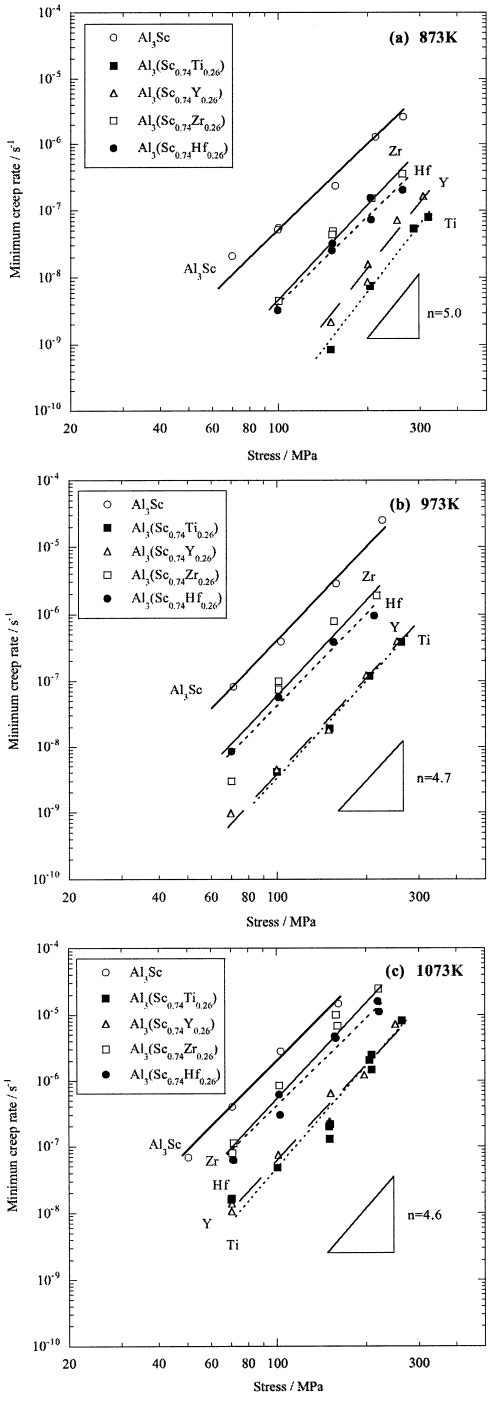

Fig. 5. Comparison of creep behavior between binary Al_3Sc and ternary $Al_3(Sc, X)$ alloys at (a) 873 K, (b) 973 K and (c) 1073 K.

For comparison, Table 4 shows that the addition of Fe to Al_3Ti increases the activation energy from 176 kJ/mol (close to the activation energy of pure Al, in agreement with the Cu_3Au rule) to about 311 kJ/mol. This increase by 136 kJ/mol is much higher than for ternary Al_3Sc and can be explained by the fact that Fe partitions to the Al sublattice, leading to an alloy with the $(Al, Fe)_3Ti$ composition. Because Fe is located on the majority sublattice which controls diffusion, its effect is much larger than in the case of $Al_3(Sc, X)$ where X is on the minority sublattice. In fact, the activation energy for creep of $(Al, Fe)_3Ti$ is close to that for self-diffusion of iron (Q = 270–282 kJ/mol [25]), as expected from the Cu_3Au rule, modified to take into account the slowest diffusing species on the majority sublattice.

4.3. Alloy design

For creep application of bulk Al_3Sc intermetallics, Ti- and Y-additions give the largest strength gain [Figs 5(a)–(c)]. Of the four solid-solution strengtheners considered in the present study, titanium has the lowest density (resulting in a modest increase of 3% as compared to binary Al_3Sc) and the lowest cost. However, as already mentioned, the Ti-containing alloys oxidize readily at 1073 K. On the other hand, yttrium gave similar creep improvements as titanium, with much better oxidation resistance and only a slightly larger mass density penalty (5% as compared to binary Al_3Sc). The larger drop in melting temperature may however be a drawback at very high temperatures, and the relatively high price of yttrium is another disadvantage.

Coarse-grained dispersion-strengthened Al-Sc-X alloys exhibit potentially attractive creep properties for aerospace or automotive structural applications at elevated temperature (up to about 600 K) [12, 36]. For the rational design of a high-temperature Al–Sc–X alloy, where the ternary alloying element

partitions completely to the Al_3Sc precipitates, the following characteristics are desirable:

1. X should have as large a solubility as possible in $L1_2$ Al_3Sc;
2. X should maximize the volume fraction of precipitate by increasing the eutectic composition and the slope of the solvus curve;
3. X should have as low a diffusion rate in Al as possible to reduce the coarsening rate of $Al_3(Sc, X)$ precipitates;
4. X should modify the lattice parameter of $Al_3(Sc, X)$, such that the lattice parameter mismatch with Al is minimized at the creep temperature to reduce coarsening rates and to delay loss of coherency;
5. X should reduce the interfacial energy of $Al_3(Sc, X)$ to reduce the coarsening rate;
6. X should strengthen the precipitates to increase resistance to shearing; and
7. X should reduce the price of the alloy.

The present work provides direct information on points (1), (4) and (6). Concerning point (1), all four elements have substantial solubility in $L1_2$ Al_3Sc. Concerning point (4), yttrium is unattractive as it increases the lattice parameter mismatch between aluminum and the $L1_2$ precipitates, while the other three elements are beneficial as they decrease the mismatch. It should be noted that segregation of X within the precipitate close to the interface with the aluminum matrix interface may significantly affect the mismatch and the interfacial energy. As to point (6), Y and Ti are superior to Zr and Hf, as already discussed above. Concerning point (3), the impurity diffusion coefficients in aluminum at 573 K are: 9.0×10^{-20} m^2/s for Sc, 6.3×10^{-24} m^2/s for Zr, 2.7×10^{-25} m^2/s for Ti [37] (no values could be found for Hf or Y in the literature). Thus, adding Ti or Zr to Al–Sc alloys will slow the growth of Al_3Sc precipitates, as reported experimentally in Al–Sc–Zr alloys [36], but titanium should be superior to zirconium given its lower diffusion coefficient in aluminum. Finally, titanium is the least expensive of the four alloying element studied [point (7)].

5. CONCLUSIONS

The compression creep behavior for binary Al_3Sc and ternary $Al_3(Sc_{0.74}X_{0.26})$, where X is Ti, Y, Zr or Hf, was studied in the temperature range 673–1200 K and the stress range 30–300 MPa. The following conclusions can be drawn:

1. $Al_3(Sc_{0.74}X_{0.26})$ alloys are essentially single-phase and show significant solid-solution strengthening. At 873 K, this corresponds to a decrease in creep

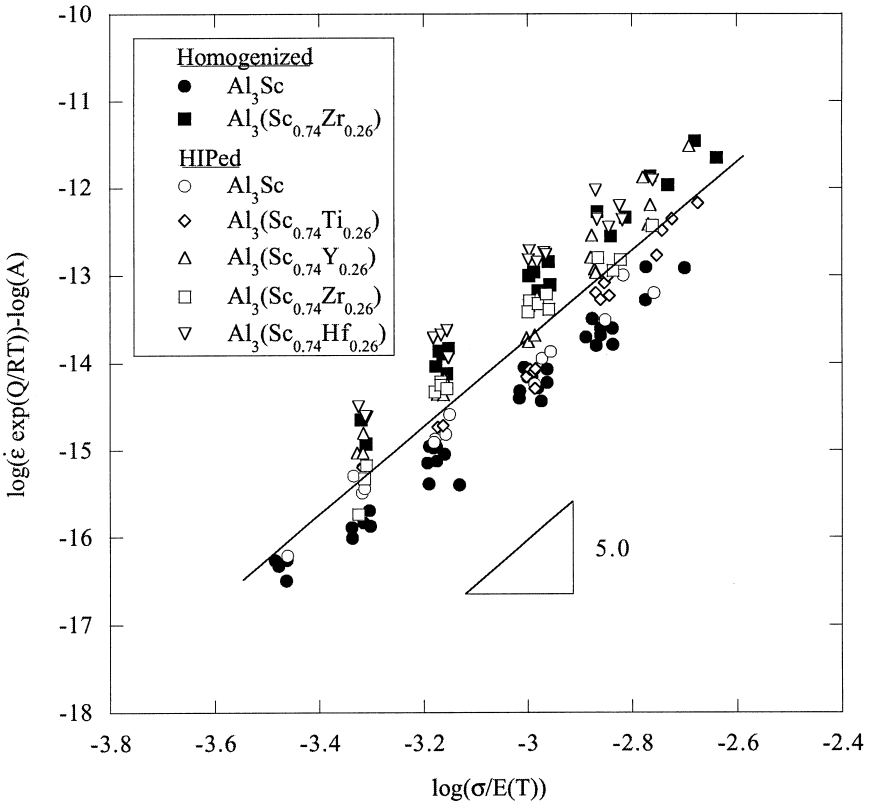

Fig. 6. Temperature-compensated plot of the minimum creep rate vs stress, showing all experimental creep data for the binary and ternary Al_3Sc alloys.

Table 4. Summary of activation energies for some trialuminides and some pure metals

Compound	Crystal structure	Composition/mol%			Activation energy, Q/kJ/mol	Temperature range/K	Method	Reference
		Hf	Al					
Al_3Hf	$D0_{22}$	25.0	75.0		184(3)	713–763	Interdiffusion	[27]
		Nb	Al					
Al_3Nb	$D0_{22}$	25.0	75.0		152(2)	1073–1573	Interdiffusion	[28]
		21.0	79.0		139–145	613–723	Interdiffusion	[29]
		Zr	Al					
Al_3Zr	$D0_{23}$	25.0	75.0		156–171	733–783	Interdiffusion	[29]
		Fe	Al					
Al_3Fe	mC102	24.9	75.1		183	1173–1358	^{26}Al radiotracer diffusivity	[30]
		V	Al					
Al_3V	$D0_{22}$	25.0	75.0		164	723–773	Interdiffusion	[31]
		Ti	Al					
Al_3Ti	$D0_{22}$	25.0	75.0		174	723–773	Interdiffusion	[31]
		25.0	75.0		178	623–748	Interdiffusion	[32]
		Ti	Al	Fe				
$(Al_{0.91}Fe_{0.09})_3Ti$	$L1_2$	24.9	68.4	6.7	309	1000–1200	Creep	[22]
$(Al_{0.884}Fe_{0.116})_{3.1}Ti$	$L1_2$	24.3	66.95	8.75	313	1000–1200	Creep	[22]
		Sc	Al	X				
Al_3Sc	$L1_2$	25.2	74.8		128(6)	673–1200	Creep	This work
$Al_3(Sc_{0.74}X_{0.26})$	$L1_2$	19.0	74.5	6.5	202(6)	873–1073	Creep	This work
Al	f.c.c.				142	729–916	^{26}Al radiotracer diffusivity	[25]
					120	512–820	NMR	[25]
Ti	α-Ti				170	1013–1149	^{44}Ti radiotracer diffusivity	[25]
					123	963–1123	^{44}Ti radiotracer diffusivity	[25]
	β-Ti				153	1173–1856	^{44}Ti radiotracer diffusivity	[25]
					131	1228–1784	^{44}Ti radiotracer diffusivity	[25]
Fe	α-Fe				282	970–1167	^{55}Fe radiotracer diffusivity	[25]
	γ-Fe				270	1337–1666	^{55}Fe radiotracer diffusivity	[25]
Y	α-Y				253	1173–1573	Mechanical sectioning	[25]
					281	1173–1573	^{91}Y radiotracer diffusivity	[25]
Zr	α-Zr				113	1013–1130	^{95}Zr radiotracer diffusivity	[25]
	β-Zr				106	1167–1476	^{95}Zr radiotracer diffusivity	[25]
					145	1218–1518	^{95}Zr radiotracer diffusivity	[25]
Hf	α-Hf				370	1470–1883	^{81}Hf radiotracer diffusivity	[25]
					349	1538–1883	Mechanical sectioning	[25]
	β-Hf				159	2012–2351	^{81}Hf radiotracer diffusivity	[25]
					183	2058–2431	^{81}Hf radiotracer diffusivity	[25]

rates of one order of magnitude for Zr and Hf, and two orders of magnitude for Ti and Y.
2. All alloys exhibit a stress exponent close to five and a short normal primary creep behavior, indicative of type II behavior characterized by the climb of dislocations.
3. The activation energies for creep is 128 ± 6 kJ/mol for Al_3Sc, close to the value of self-diffusion for pure Al, as expected from the "Cu_3Au rule". Activation energies for ternary alloys are all about 202 kJ/mol, indicating that diffusion on the Al sublattice is hampered by lattice strain introduced by the alloying elements.
4. Among the four alloying elements investigated, titanium seems the best candidate as a potential addition to dilute Al–Sc alloys, based on its high strengthening capability and relatively low melting point depression of Al_3Sc, and its low density and price. For bulk Al_3Sc applications, Y may be better due to its much better oxidation resistance, but it induces a relatively large melting-point depression.

Acknowledgements—This research was supported by the Division of Materials Sciences, United States Department of Energy under contract DE-FG02-98ER45721. Y.H. greatly appreciates the support of the Japan Society for the Promotion of Science for Young Scientists in the form of a Research Fellowship. The authors also acknowledge Professors M. Asta and D. N. Seidman (Northwestern University) for useful discussion, Professor Y. Matsumoto (Oita National College of Technology) for electrode-discharge-machining the creep specimens and Mr Y. Sasaki (Nagoya University) for performing the calorimetric measurements.

REFERENCES

1. George, E. P., Pope, D. P., Fu, C. L. and Schneibel, J. H., *ISIJ International*, 1991, **31**, 1063.
2. Yamaguchi, M., Umakoshi, Y. and Yamane, T., in *High Temperature Ordered Intermetallic Alloys II*, ed. N. S. Stoloff, C. C. Koch, C. T. Liu and O. Izumi. MRS, **81**, 1986, 275.
3. Schneibel, J. H. and Porter, W. D., in *High Temperature Ordered Intermetallic Alloys III*, ed. C. T. Liu, A. I. Taub, N. S. Stoloff and C. C. Koch. MRS, **133**, 1988, 335.
4. Srinivasan, S., Desch, P. B. and Schwarz, R. B., *Scripta metall. mater*., 1991, **25**, 2513.
5. Foley, J. C., Perepezko, J. H. and Skinner, D. J., *Mater. Sci. Engng*, 1994, **A179/A180**, 205.
6. Nic, J. P., Zhang, S. and Mikkola, D. E., in *High Temperature Ordered Intermetallic Alloys IV*, ed. L. A. Johnson, D. P. Pope and J. O. Stiegler. MRS, **213**, 1990, 697.
7. Zhang, S., Nic, J. P. and Mikkola, D. E., *Scripta metall. mater*., 1990, **24**, 57.
8. Schneibel, J. H., Horton, J. A. and Porter, W. D., *Mater. Sci. Engng*, 1992, **A152**, 126.
9. Fukunaga, K., Shouji, T. and Miura, Y., *Mater. Sci. Engng*, 1997, **A239–A240**, 202.
10. Schneibel, J. H. and Hazzledine, P. M., *J. Mater. Res*., 1992, **7**, 868.
11. Flower, H. M., *High Performance Materials in Aerospace*. Chapman & Hall, 1995.
12. Fuller, C. B., Seidman, D. N. and Dunand, D. C., *Scripta mater*, 1999, **40**, 691.
13. Hyland Jr, R. W., *Metall. Trans*., 1992, **23A**, 1947.
14. George, E. P., Horton, J. A., Porter, W. D. and Schneibel, J. H., *J. Mater. Res*., 1990, **5**, 1639.
15. Schneibel, J. H. and George, E. P., *Scripta metall. mater*., 1990, **24**, 1069.
16. Drits, M. E., Toropova, L. S., Gushchina, F. L. and Fedotov, S. G., *J. Soviet Non Ferrous Metal. Res*., 1984, **12**, 83.
17. Murray, J. L., *Binary Alloy Phase Diagrams*. American Society for Metals, Metals Park, OH, 1986.
18. Kassner, M. E. and Perez-Prado, M., *Prog. Mater. Sci*., 2000, **45**, 1.
19. Wolfenstine, J., Kim, H. K. and Earthman, J. C., *Scripta metall. mater*., 1992, **26**, 1823.
20. Hemker, K. J. and Nix, W. D., *Metall. Trans*., 1993, **24A**, 335.
21. Hayashi, T., Shinoda, T., Mishima, Y. and Suzuki, T., in *High Temperature Ordered Intermetallic Alloys IV*, ed. L. A. Johnson, D. P. Pope and J. O. Stiegler. MRS, **213**, 1990, 617.
22. DiPietro, M. S., Kumar, K. S. and Whittenberger, J. D., *J. Mater. Res*., 1991, **6**, 530.
23. Hyland, R. W. and Stiffler, R. C., *Scripta metall. mater*., 1991, **25**, 473.
24. Barrett, C. R., Ardell, A. J. and Sherby, O. D., *Trans. Metall. Soc., AIME*, 1964, **230**, 200.
25. Mehrer. H. (ed.) *Diffusion in Solid Metals and Alloys*, Springer Verlag, 1990.
26. d'Heurle, F. M., Gas, P. and Philibert, J., *Solid State Phenomena*, 1995, **41**, 93.
27. Ball, R. K., Freeman, W. G. and Todd, A. G., *Thin Solid films*, 1988, **161**, 235.
28. Ogútani, T., *Metal. Trans*., 1972, **3**, 421.
29. Ball, R. K. and Todd, A. G., *Thin Solid films*, 1987, **149**, 269.
30. Larikov, L. N., Geichenko, V. V. and Fal'chenko, V. M., *Diffusion Processes in Ordered Alloys*. Naukova Dumka Publisher, Kiev, 1975.
31. Nakamura, K., Lau, S. S., Nicolet, M.-A. and Mayer, J. W., *App. Phys. Lett*., 1976, **28**, 277.
32. Tardy, J. and Tu, K. N., *Phys. Rev. B*, 1985, **32**, 2070.
33. Nonaka, K., Arayashiki, T., Nakajima, H., Almazouzi, A., Tanaka, K., Ikeda, T., Numakura, H. and Koiwa, M., *Defect and Diffusion Forum*, 1997, **143–147**, 269.
34. Frank, S., Söervall, U. and Herzig, C., *Phy. Status Solidi B*, 1995, **191**, 45.
35. Takesue, H., Oh-ishi, K., Horita, Z. and Nemoto, M., *Mater. Sci. Engng*, 1997, **A239–A240**, 479.
36. Toropova, L. S., Eskin, D. G., Kharakterova, M. L. and Dobatkina, T. V., *Advanced Aluminum Alloys Containing Scandium*. Gordon and Breach Science Publisher, 1998.
37. Fujikawa, S., *Defect and Diffusion Forum*, 1997, **143–147**, 115.